H.G.K.G. Jayatunga, B.T. Tan, J. S. Leontini

Abstract

Keywords: Fluid-structure interaction, transverse galloping.

1. Selection of the cross section

The cross section selection process for this study was based to three key criteria

- The cross section should have a bluff front face with sharp upstream corners for the flow to separate at the leading edges;
- As the proximity of shear layers to the body plays a vital role in creating C_y (**?**), the cross section should have a basic level of streamlining.
- The cross section should consist of a geometric profile in the afterbody, to inhibit or delay the shear layer reattachment.

The square cross section which has been widely used in galloping studies satisfies the first two selection criteria. Thus, a modification to the square cross section was done in order to meet the third criterion. Thus, in order to inhibit the shear layer reattachment, the top and bottom sides of the trailing edges of the square were tapered off and a hybrid cross section of a rectangle and a triangle (illustrated in figure 1), i.e, a pentagon was produced.

The inhibition of the shear layer can be varied systematically by varying one parameter, $\frac{d}{l}$; which was an advantage of this cross section. The ratio $\frac{d}{l}$ was varied from 1 to zero in increments of 0.25 where 1 is the square cross section and 0 is an isosceles triangle.

2. Static body results

Stationary time averaged C_y results were obtained for cross sections where $\frac{d}{l}$ = 1, 0.75 ,0.5, 0.25 and 0 using DNS at Re = 200. Table 1 shows the coefficients of the 7^{th} order curve fitting for each cross section. To achieve a

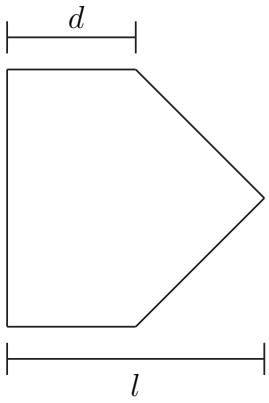

Figure 1: Illustration of the hybrid cross section (combination of a square and a triangle) obtained by tapering the afterbody of the square. The afterbody was changed by changing the ratio of $\frac{d}{l}$. Hence, data were obtained for $\frac{d}{l} = 1, 0.75, 0.5, 0.25$ and 0 were considered in this study.

better fit, piecewise interpolation using multiple $7th$ order polynomials were incorporated for a single cross section, giving more importance to accurately fitting the positive portion of the C_y curve; as the power transfer from the fluid to the body only occurs in this region.

The C_y vs. θ curves in figure 2 show the resultant of the piecewise curve-fits obtained for each cross section. A shift of the peak value of C_y to the right can be observed as the $\frac{d}{l}$decreases therefore, the peak C_y occurs at higher induced angles. The overall trends of this behaviour agrees with trends of **?** where the peak C_y value was shifted to higher induced angles when reattachment was delayed on a trapezoidal body. The peak value of C_y occurs at high induced velocities as $\frac{d}{l}$ is decreased because θ is proportional to the transverse velocity of the body via $\tan\theta = \frac{\dot{y}}{U}$. Thus, these bodies with a short straight section, or small $\frac{d}{l}$, satisfy one of the three conditions required to optimize the power transfer.

A negative region could be observed on the $C_y$vs. θ curves where $\frac{d}{l} \leq 0.25$

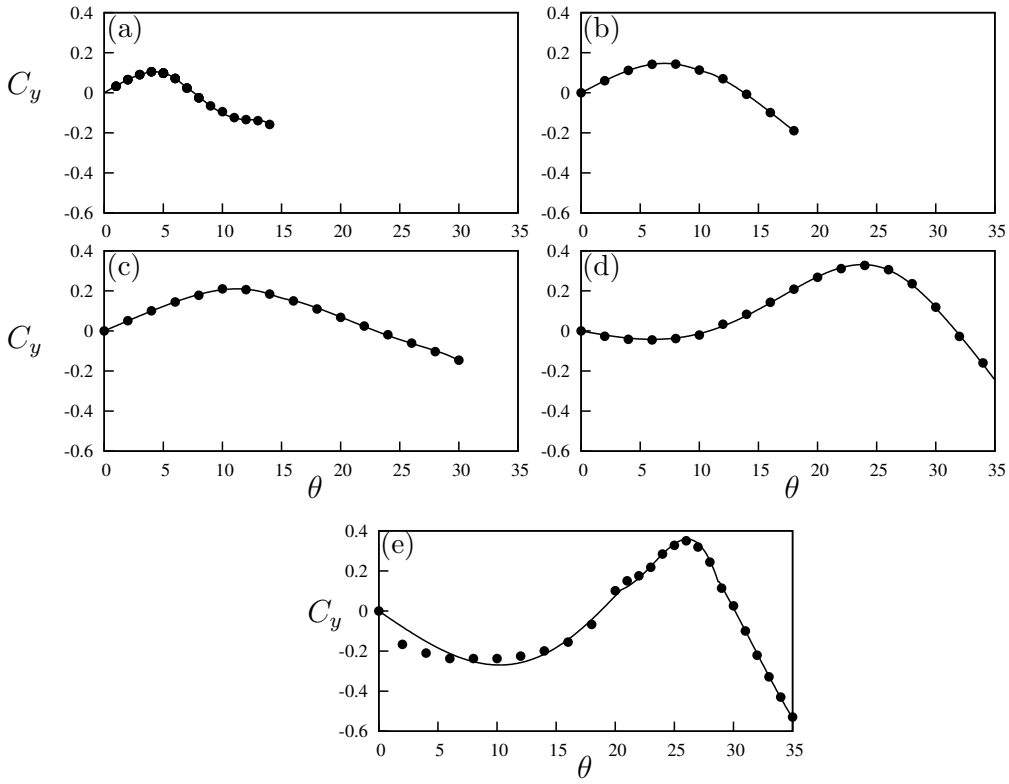

Figure 2: Induced lift coefficient C_y at different angles for selected cross sections. Data presented for cross sections, (a) square, (b) $\frac{d}{l} = 0.75$, (c) $\frac{d}{l} = 0.5$, (d) $\frac{d}{l} = 0.25$ and (e) triangle. Points ($\bullet$) are predicted from the static body simulations and the curves are the compound 7^{th} order polynomials.

$\frac{d}{l}$	a_1	a_3	a_5	a_7	Overlap range
0	-2.30617	-269.075	-59.2929	4.74389	$20.5^\circ - 23.5^\circ$
	-5.08342	-56.5390	-160.505	-105.773	$28.6^\circ - 28.7^\circ$
	4.40685	19.9213	22.8894	7.68556	
0.25	-0.605146	-19.4346	-82.4463	-94.4226	$30.1^\circ - 30.2^\circ$
	2.50538	9.91021	10.2712	3.94112	
0.5	1.44734	4.83885	-166.900	-983.072	$14^\circ - 16^\circ$
	1.51455e	15.8476	52.5465	62.8067	
0.75	1.76938	35.2630	-345.562	-10072.7	$11.03^\circ - 11.11^\circ$
	1.77553	43.0120	262.983	638.484	

Table 1: Coefficient values used in the 7th order interpolation polynomial at $Re = 200$. Data present for $\frac{d}{l} = 0 - 0.75$ at increments of 0.25. Multiple polynomials were used to attain a better fit. The plot of the compound fit is presented in figure 2. The "Overlap" range refers to the range of angles which the transition of the two polynomials take place.

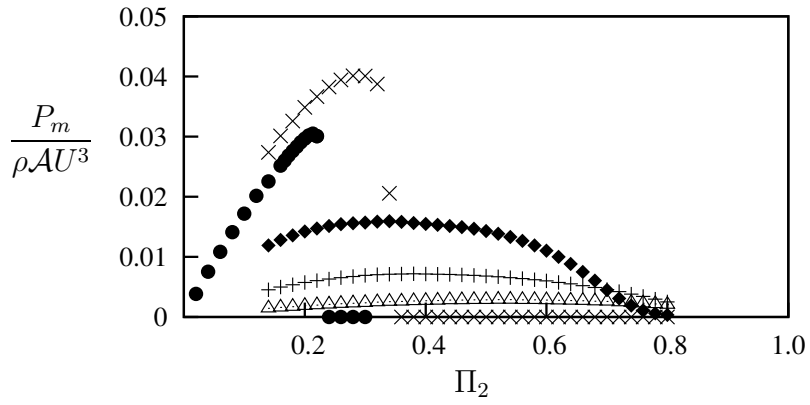

Figure 3: Dimensionless mean power obtained using QSS model as a function of Π_2. Data presented for five selected cross sections, square (△), $\frac{d}{l} = 0.75$ (+), $\frac{d}{l} = 0.5$ (◆), $\frac{d}{l} = 0.25$ (×) and triangle (●) at $Re = 200$, $\Pi_1 = 100$.

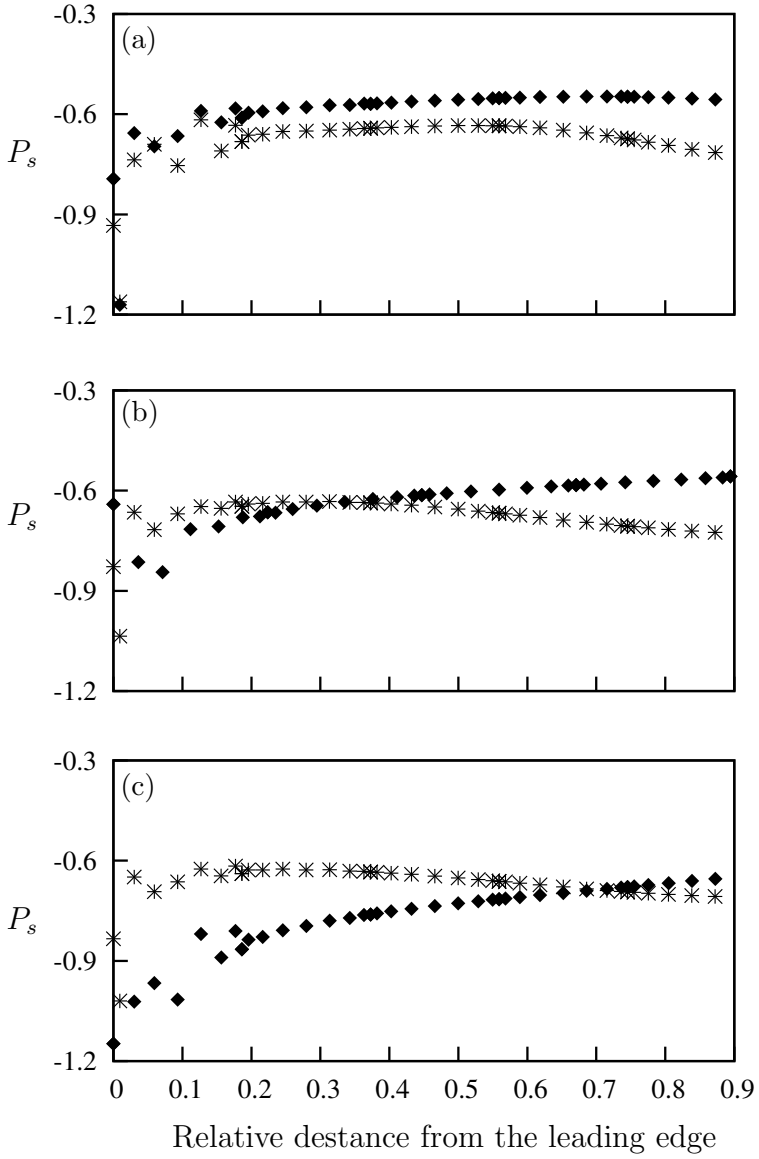

Figure 4: Surface pressure of top (✳) and bottom (◆) surfaces of the static triangular cross section at (a) $\theta = 4°$, (b) $\theta = 16°$ and (c) $\theta = 21°$ A clear pressure difference is visible between the top and bottom surfaces. The top surface comparatively has more negative pressure compared to the bottom surface and reduces as θ is increased and vice versa occurs at the bottom surface. Thus, initially the effective force is upwards which results in a negative C_y. The effective C_y becomes positive as θ is increased.

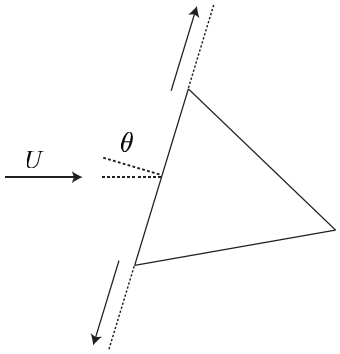

Figure 5: Illustration of the lines along which the flow velocity magnitudes have been extracted. The data have been extracted along a line starting from the separation points in the outward direction (shown with arrows) for the top and bottom surfaces.

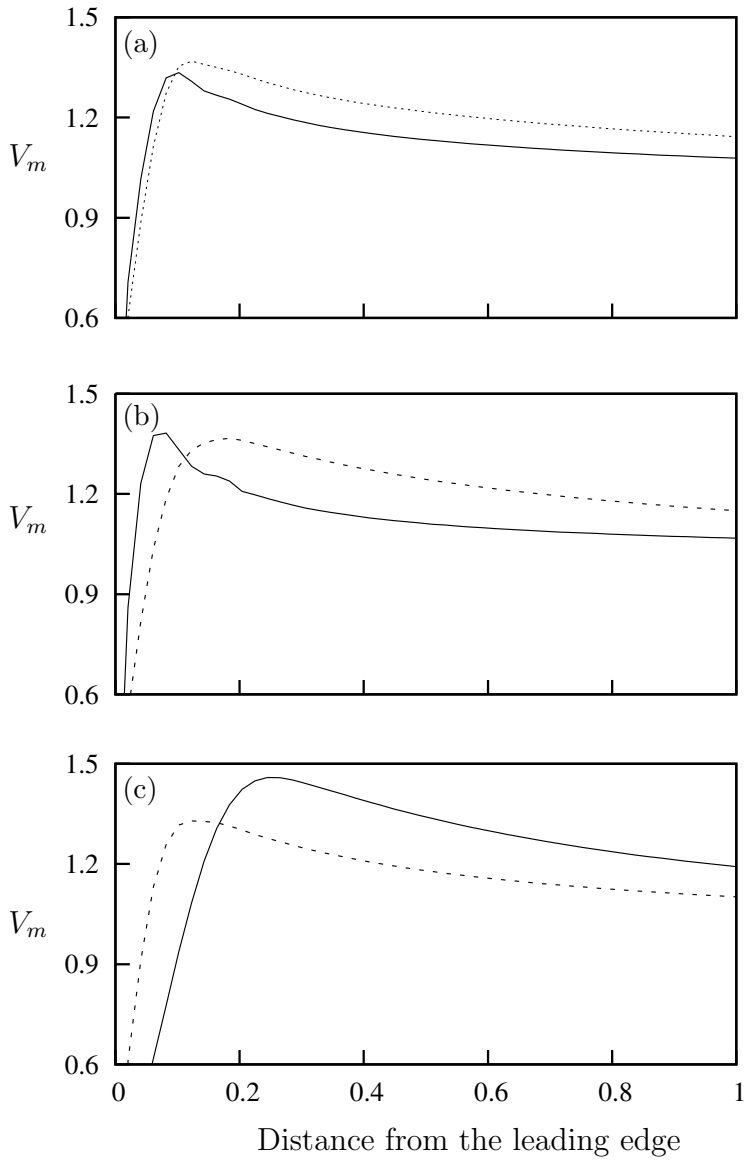

Figure 6: Velocity magnitudes of the flow along a line parallel to the front surface spreading towards top (- - -) and bottom (———) boundaries (figure 5). These two lines (for the top and bottom surfaces) start from the top and bottom leading edges of the triangular cross section. Data present (a) $\alpha = 4°$, (b) $\alpha = 16°$ and (c) $\alpha = 21°$.

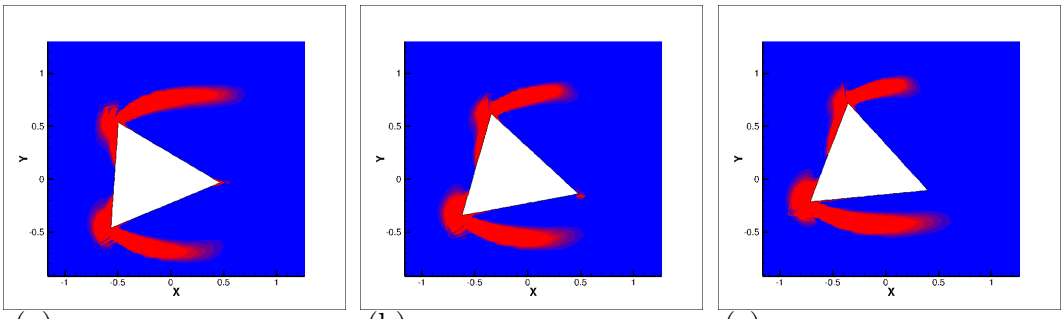

Figure 7: Contours of the magnitude of the shear strain rate of time averaged flow field on the stationary isosceles triangle ($\frac{d}{l} = 0$) at $Re = 200$ at different incidence angles. (a) 4° (negative value of C_y that is further decreasing with increasing θ), (b) 16° (negative value of C_y that is increasing with increasing θ) and (c) 21° (a significantly positive value of C_y). The bottom shear layer comes closer to the bottom wall and as the angle of incidence increases.

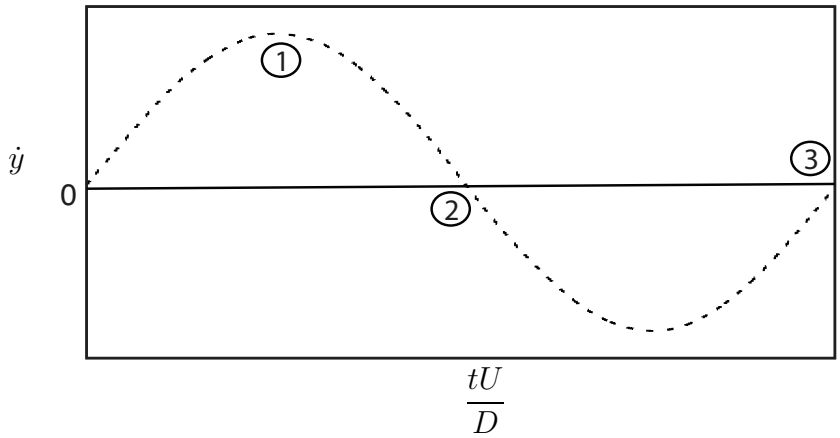

Figure 8: Illustration of the time history of velocity depicting the points considered to obtained time averaged stream traces. The points considered are: point 1 where $\dot{y}$ is maximum, point 2 where $\dot{y}$ is close to zero with a negative gradient and point 3 where $\dot{y}$ is close to zero with a positive gradient.

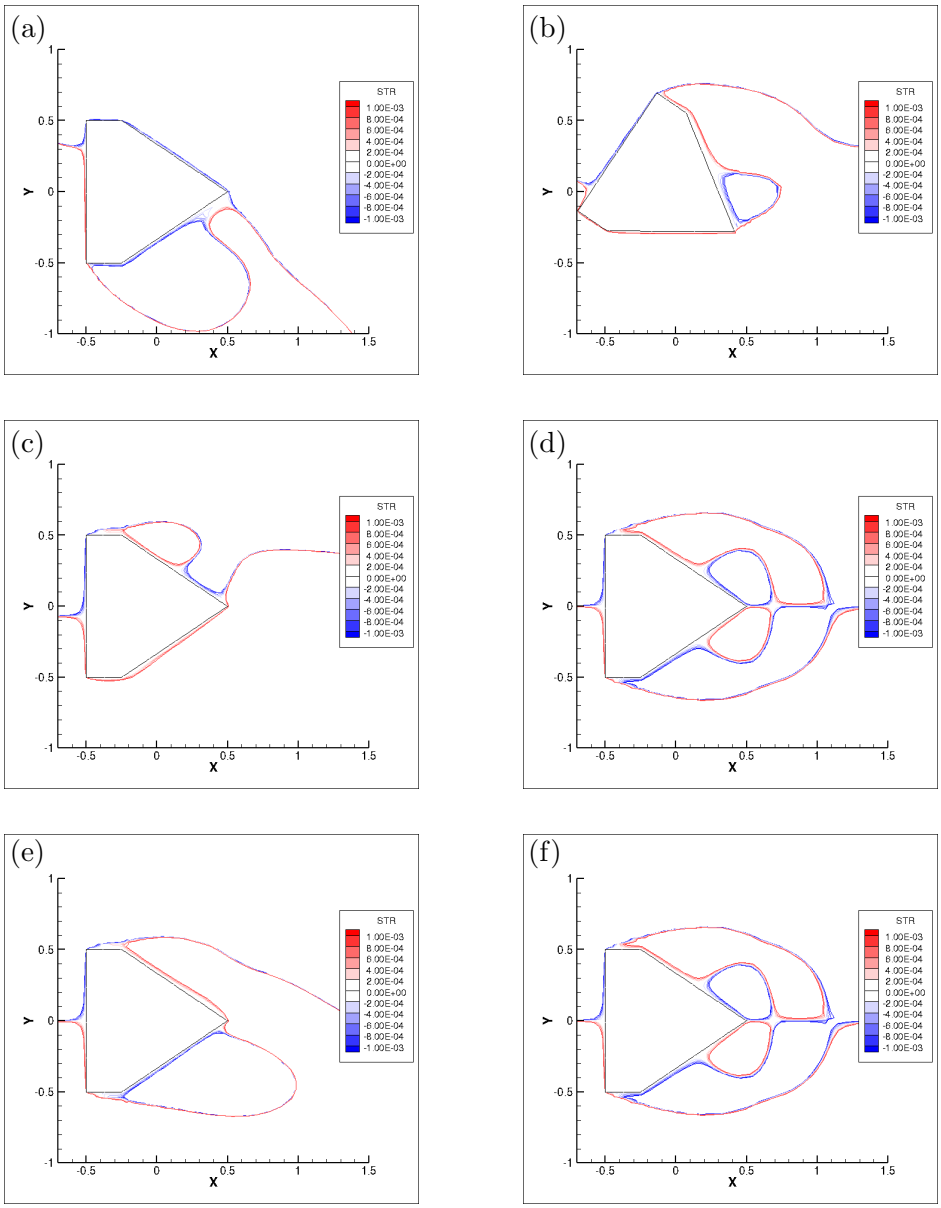

Figure 9: Time averaged stream functions of stationary and oscillating flow-fields of the hybrid cross section ($\frac{d}{l} = 0.25$), averaged over a vortex shedding cycle. (a), (c) and (e) are the averaged stream functions of the oscillating case at $\frac{tU}{D} = 2295.763$ (point 1), $\frac{tU}{D} = 2305.897$ (point 2) and $\frac{tU}{D} = 2325.870$ (point 3) . (b), (d) and (f) are the stream functions of the flow field of the stationary body corresponding to the induced angles of (a), (c) and (e).